Precision Engineering 45 (2016) 311–321

Contents lists available at ScienceDirect

Precision Engineering

journal homepage: www.elsevier.com/locate/precision

Mechanistic force model coefficients: A comparison of linear regression and nonlinear optimization

Mark A. Rubeo, Tony L. Schmitz*

University of North Carolina at Charlotte, Mechanical Engineering and Engineering Science Department, 9201 University City Boulevard, Charlotte, NC 28223, USA

ARTICLE INFO

Article history:
Received 23 October 2015
Accepted 13 March 2016
Available online 19 March 2016

Keywords:
Milling
Stability
Chatter
Force
Model
Coefficients
Regression
Optimization

ABSTRACT

This paper describes a comparative study devised to examine the dependence of specific force coefficients, which are used in mechanistic cutting force models, on various milling process parameters such as feed per tooth, spindle speed, milling configuration, and radial immersion. Two methods are described for determining the specific force coefficients: (1) the average force, linear regression method; and (2) the instantaneous force, nonlinear optimization method. A series of test cuts were performed and the specific force coefficients calculated using the two methods were compared. Additionally, a technique for extending the bandwidth over which the cutting forces were measured using a commercially available cutting force dynamometer is presented. Finally, a series of milling stability experiments were conducted to validate the calculated specific force coefficients. It was found that milling process parameters such as feed per tooth, spindle speed, and radial immersion exhibit a nonlinear relationship with the specific force coefficients.

1. Introduction

The modeling of machining processes, which has been an important research topic for nearly a century, is motivated by the requirements of both machine tool users and builders. The machine tool user aims to reliably predict key process outputs, including cutting forces which affect workpiece surface quality, workpiece geometric accuracy, and process stability. From the builder's perspective, the cutting forces represent a critical design metric because they dictate the required spindle power and torque as well as the required rigidity of the machine tool's structural loop. In machining process simulations and optimizations, cutting force modeling strongly affects the accuracy of the results.

There are three approaches to cutting force modeling which are described in the literature: analytical, numerical, and mechanistic [1,2]. The analytical models relate cutting forces to a number of process variables (i.e., feed per tooth, cutting speed, and cut geometry) and mechanical aspects such as shear angle, material properties, and friction. Early work using this approach was detailed by Merchant in [3] and by Amarego and Brown in [4]. Increased computational power has led to advancements in numerical modeling, where the relationship between chip and tool geometry is studied [5].

The mechanistic force models assume that the instantaneous cutting forces are proportional to the uncut chip area through one or more empirical coefficients [1]. Early work in mechanistic force modeling for milling operations was reported by Martellotti [6], Koenigsberger et al. [7], and Sabberwal [8]. The literature highlights two primary mechanistic force models. The first relates instantaneous cutting forces and uncut chip areas to a single empirical coefficient which is commonly referred to as the specific (cutting) force coefficient, K_S. This coefficient captures the effect of both cutting (shearing) and ploughing (due to friction at the cutting edge) which occurs during chip formation. The ease of implementation and predictive capabilities provided by this simple model have resulted in its widespread application in industry and research. The second, published in later works by Budak et al. [9], extends the mechanistic cutting force model to include separate empirical coefficients to capture the chip formation mechanics of shearing and ploughing.

In [10,11], a method for the identification of the empirical coefficients, commonly referred to as specific force coefficients, is presented. The procedure proposes that a linear regression of measured cutting forces be performed over a range of feed per tooth values while holding other process parameters such as cutting speed and cut geometry constant. This method, which requires several cutting tests to perform the linear regression analysis, provides

* Corresponding author. Tel.: +1 7046875086.
E-mail address: tony.schmitz@uncc.edu (T.L. Schmitz).

http://dx.doi.org/10.1016/j.precisioneng.2016.03.008
0141-6359/

results which are specific to the selected cutting tool geometry and workpiece material combination. The regression analysis assumes that the cutting forces are linearly dependent on feed per tooth and independent of other machining parameters such as cutting speed and feed, cut geometry, and cut direction (i.e., up milling/down milling). Other methods, such as those presented in [12,13], use nonlinear optimization methods to perform a least squares fit of simulated cutting forces to measured cutting forces. This approach requires measurements from a single cutting test and, again, results in specific force coefficients which are specific to the chosen machining parameters. As such, the specific force coefficients may be considered to be a function of not only the cutting tool geometry and workpiece material, but also machining parameters, such as cutting speed, feed, cut geometry, and cut direction. The nonlinear optimization method provides a tool for studying the effects of these machining parameters on dynamic cutting forces.

It has been demonstrated in the literature that the measurement of cutting forces with piezoelectric dynamometers at high cutting speeds is complicated by the dynamic influence of the instrument. As the tooth passing frequency and subsequent harmonics exceed the dynamometer bandwidth (i.e., the frequency range over which the frequency response is nominally constant) spurious frequency content is superimposed on the measured cutting forces. In [14] Altintas et al. use a Kalman filtering approach to remove the dynamic influence of a novel spindle-integrated force sensor's structural modes. Other research, such as that presented in [15–24], has also addressed the challenges associated with limited dynamometer bandwidth using force-to-force frequency response function (FRF) measurement, filtering, and other techniques.

In this paper, a comparative study is described where the specific force coefficients of the mechanistic force model are determined using both linear regression and nonlinear optimization methods. The paper is organized as follows. First, the mechanistic force model is detailed, and the two methods for specific force coefficient determination are described. Next, the experimental method, which includes the cutting force measurement, the dynamic compensation technique, and the stability testing setup, is detailed. Finally, the resultant cutting force coefficients are compared and the practicality of the nonlinear optimization method is demonstrated in the framework of a milling stability prediction via time domain simulation and experimental validation. This is followed by a discussion of the experiment results and their impact on finish milling operations at low radial immersion.

2. Mechanistic force modeling

The mechanistic force models are based on the assumptions that: (1) the instantaneous cutting force is proportional to the cross sectional area of the uncut chip through empirical specific force coefficients; and (2) the instantaneous cutting forces are independent of other machining parameters. Although these assumptions provide a reasonable degree of accuracy for milling stability prediction using stability lobe diagrams [10], it has been shown that cutting forces are dependent on cutting speed and feed [13]. The mechanistic force model used in this study includes instantaneous cutting forces in the tangential, F_t, normal, F_n, and axial, F_a, directions with six corresponding force coefficients; see Eqs. (1)-(3):

$$F_t = k_{tc} b h + k_{te} b \tag{1}$$

$$F_n = k_{nc} b h + k_{ne} b \tag{2}$$

$$F_a = k_{ac} b h + k_{ae} b \tag{3}$$

where b is the chip width (i.e., axial depth of cut in milling) and h is the instantaneous chip thickness, which is based on the circular tooth path approximation; see Eq. (4):

$$h = f_t \sin(\phi) \tag{4}$$

where f_t is the feed per tooth and ϕ is the cutter rotation angle. Each component of the instantaneous cutting force includes two specific force coefficients. The coefficients k_{tc}, k_{nc}, and k_{ac} are correlated with cutting and the edge coefficients k_{te}, k_{ne}, and k_{ae} are correlated with ploughing. The edge coefficients affect the instantaneous cutting force proportionally through the chip width, but are independent of the instantaneous chip thickness.

2.1. Average force, linear regression method

The six specific force coefficients were determined through linear regression analysis using the average cutting forces measured during a series of cutting tests which were performed over a range of feed per tooth values while holding other milling parameters constant. Projecting the tangential, normal, and axial cutting force components into a fixed reference frame (i.e., x, y, and z), shown in Fig. 1, and averaging over one cutter revolution yields the following expressions for mean cutting force per revolution.

$$\bar{F}_x = \left\{ \frac{N_t b f_t}{8\pi}[-k_{tc}\cos(2\phi) + k_{nc}(2\phi - \sin(2\phi))] + \frac{N_t b}{2\pi}[k_{te}\sin(\phi) - k_{ne}\cos(\phi)] \right\}_{\phi_s}^{\phi_e} \tag{5}$$

$$\bar{F}_y = \left\{ \frac{N_t b f_t}{8\pi}[k_{tc}(2\phi - \sin(2\phi)) + k_{nc}\cos(2\phi)] - \frac{N_t b}{2\pi}[k_{te}\cos(\phi) + k_{ne}\sin(\phi)] \right\}_{\phi_s}^{\phi_e} \tag{6}$$

$$\bar{F}_z = \left\{ \frac{N_t b}{2\pi}[k_{ac} f_t \cos(\phi) - k_{ae}\phi] \right\}_{\phi_s}^{\phi_e} \tag{7}$$

where N_t is the number of teeth on the cutter and ϕ_s and ϕ_e are the start and exit angles of each tooth based on the radial depth of cut and cut direction.

Often, 100% radial immersion (i.e., slotting) cutting tests are selected, where $\phi_s = 0^\circ$ and $\phi_e = 180^\circ$, so that the mean cutting force per revolution expressions simplify to:

$$\bar{F}_x = \frac{N_t b k_{nc}}{4} f_t + \frac{N_t b k_{ne}}{\pi} \tag{8}$$

$$\bar{F}_y = \frac{N_t b k_{tc}}{4} f_t + \frac{N_t b k_{te}}{\pi} \tag{9}$$

$$\bar{F}_z = -\frac{N_t b k_{ac}}{\pi} f_t - \frac{N_t b k_{ae}}{2} \tag{10}$$

These expressions are provided in slope–intercept form. A linear regression over feed per tooth may be performed to determine the cutting force coefficients. The slope, a_{1j}, and intercept, a_{0j}, of the linear regression are given as:

$$a_{1j} = \frac{n\sum_n^{i=1} f_{t,i}\bar{F}_{j,i} - \sum_n^{i=1} f_{t,i}\sum_n^{i=1}\bar{F}_{j,i}}{n\sum_n^{i=1} f_{t,i}^2 - \left(\sum_n^{i=1} f_{t,i}\right)^2} \tag{11}$$

$$a_{0j} = \frac{1}{n}\sum_{i=1}^{n}\bar{F}_{j,i} - a_{1j}\frac{1}{n}\sum_{i=1}^{n} f_{t,i} \tag{12}$$

where j indicates the force component direction (i.e., x, y, or z) and n is the number of data pairs ($f_{t,i}$, $\bar{F}_{j,i}$). Once the slope and intercept

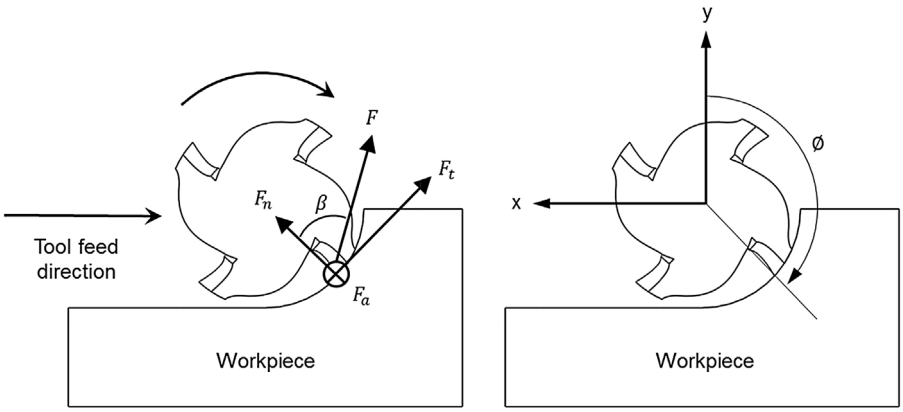

Fig. 1. Force components and fixed reference frame for the average force, linear regression method. A down milling configuration is shown with a helical endmill.

are determined, the specific coefficients are calculated using Eqs. (13)–(15).

$$k_{tc} = \frac{4a_{1y}}{N_t b} k_{te} = \frac{\pi \cdot a_{0y}}{N_t b} \tag{13}$$

$$k_{nc} = \frac{4a_{1x}}{N_t b} k_{ne} = \frac{\pi \cdot a_{0x}}{N_t b} \tag{14}$$

$$k_{ac} = -\frac{\pi \cdot a_{1z}}{N_t b} k_{ae} = -\frac{2a_{0y}}{N_t b} \tag{15}$$

The derivation of the specific cutting force coefficients for the general case of arbitrary radial immersion is given in Appendix A.

2.2. Instantaneous force, nonlinear optimization method

Alternatively, the cutting force coefficients were determined using an instantaneous force, nonlinear optimization method which solves a nonlinear, least squares curve fitting problem and takes into account the user-defined lower and upper bounds on the decision variables (i.e., specific force coefficients and flute-to-flute runout). The optimization routine, which uses a trust-region-reflective least squares algorithm, equates cutting forces simulated in the time domain with measured cutting forces at each discrete time step.

The time domain simulation calculates the cutting forces at each small time step, dt, which is defined in the simulation as:

$$dt = \frac{1}{f_s} \tag{16}$$

where f_s is the sampling frequency of the cutting force measurement. At each time step the instantaneous chip thickness is computed, the cutting force is calculated, the tooth angle, ϕ, is incremented by a small angle, $d\phi$, which depends on the spindle speed and the time step, and the process is repeated for one complete revolution of the cutting tool. The instantaneous chip thickness is determined using the circular tooth path approximation and assuming a rigid tool and workpiece. Additionally, flute-to-flute runout of the cutting tool is incorporated into the instantaneous chip thickness calculation. For a more thorough and robust model, the actual trochoidal tooth path [25], which more accurately models the instantaneous chip thickness at the start and exit of the cut, may be employed. However, in this study the circular tooth path approximation provided adequate accuracy at significantly lower computational cost. Because the instantaneous force, nonlinear optimization method is capable of solving nonlinear curve fitting problems, the mechanistic force model may be modified to include a nonlinear dependence on chip thickness which was presented by Feng et al. [26] for ball endmilling processes.

The tangential, F_t, normal, F_n, and axial, F_a, cutting force components were calculated according to the mechanistic force model defined in Section 2. In order to represent the simulated forces in the fixed reference frame of the measured cutting forces, a coordinate transformation was performed:

$$\begin{Bmatrix} F_x \\ F_y \\ F_z \end{Bmatrix}_{simulated} = \begin{bmatrix} \cos(\phi) & \sin(\phi) & 0 \\ \sin(\phi) & -\cos(\phi) & 0 \\ 0 & 0 & 1 \end{bmatrix} \begin{Bmatrix} F_t \\ F_n \\ F_a \end{Bmatrix}_{simulated} \tag{17}$$

where ϕ is the instantaneous cutter rotation angle. The objective function was defined as:

$$f_i(k) = \begin{Bmatrix} F_x \\ F_y \\ F_z \end{Bmatrix}_i^{simulated} - \begin{Bmatrix} F_x \\ F_y \\ F_z \end{Bmatrix}_i^{measured} \tag{18}$$

where k is the vector of decision variables, which includes the six specific force coefficients and the flute-to-flute runout of the cutting tool, and $f_i(k)$ is the difference between the x, y, and z components of the instantaneous simulated and measured cutting forces at the ith time step.

Because the time step between each simulated instantaneous cutting force must coincide with the measured cutting forces, the size of the resulting system of equations depends on the sampling frequency of the measurement and the number of cutting tool revolutions (i.e., number of time steps) included in the optimization. The nonlinear, least squares curve fitting problem takes the form:

$$\min_k \left\| f(k) \right\|_2^2 = \min_k (f_1(k)^2 + f_2(k)^2 + \cdots + f_n(k)^2) \tag{19}$$

where n is the number of time steps. The curve fitting problem is solved via a trust-region-reflective algorithm, which is based on an interior-reflective Newton approach that is well suited for solving nonlinear optimization problems where the decision variables are bounded by upper and/or lower limits [27].

For this study, the measured cutting forces were partitioned into 100 individual revolutions of the cutting tool and averaged; see Fig. 2. The measured cutting forces exhibited a high degree of repeatability from one revolution of the cutting tool to the next. The average measured cutting force components were then used for the nonlinear optimization function along with a number of relevant process parameters, including the number of teeth on the cutting tool, sampling frequency of the force measurement, and initial guesses for the decision variables (i.e., specific force coefficients and flute-to-flute runout).

The optimization function simulates the instantaneous cutting forces in the x, y, and z directions based on the input process

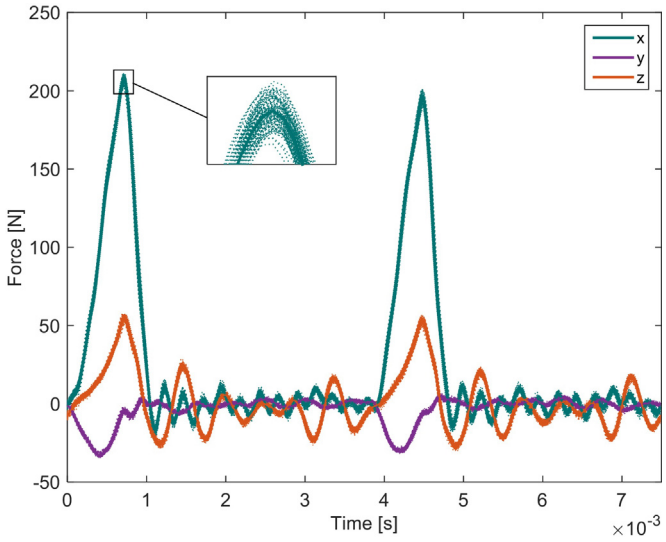

Fig. 2. Measured cutting forces over 100 revolutions of the cutting tool (dotted line) and their average (solid line) shown for a milling operation using a 2-flute cutting tool.

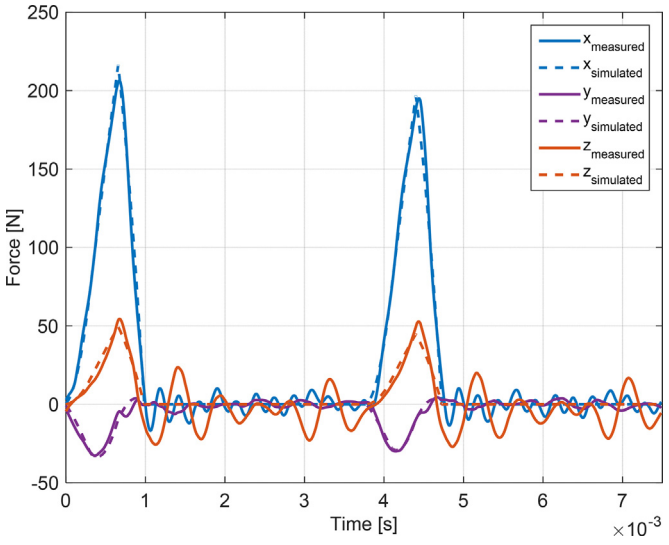

Fig. 3. Example results from the nonlinear, optimization method including the measured cutting forces and optimized, simulated cutting forces.

parameters. The difference between the simulated and measured cutting forces is then calculated by the objective function given in Eq. (18) and the sum of squares of the differences are evaluated. The evaluation is then scrutinized against an arbitrary, user-defined set of convergence criteria, such as the change in the sum of the squares from one iteration to the next. If it is determined that the convergence criteria are met, the optimization routine ceases; otherwise, the decision variables are updated and the process iterates until convergence. Example results of the optimized, simulated cutting forces are shown in Fig. 3. Good agreement between the measured and simulated cutting forces are observed.

3. Experimental method

The process parameter dependence of the specific force coefficients was investigated using both the average force, linear regression and instantaneous force, nonlinear optimization methodologies. A series of cutting tests were performed and the cutting forces were measured. Because the tooth passing frequency was sufficiently high that the measured cutting forces suffered dynamic distortions due to the limited measurement bandwidth of the dynamometer, the measured cutting forces were compensated to attenuate the spurious frequency content. The compensated cutting forces were then analyzed using the two methods and the resulting specific force coefficients were used to make stability predictions based on time domain simulations. A pictorial illustration of the experimental method used in the study is displayed in Fig. 4.

3.1. Cutting force measurement setup

Cutting tests were performed on a LeBlond Makino A55 Plus horizontal milling machine with a maximum spindle speed of 20,000 rpm. The workpiece material was aluminum 6061-T6511 extruded barstock with approximate dimensions of 170 mm × 100 mm × 38 mm. It was rigidly fixed to the three-component cutting force dynamometer (Kistler 9257B) via two M8 socket head cap screws; see Fig. 5. The dynamometer/workpiece combination was bolted to the machine tool's tombstone via a surface ground steel plate approximately 25 mm in thickness and

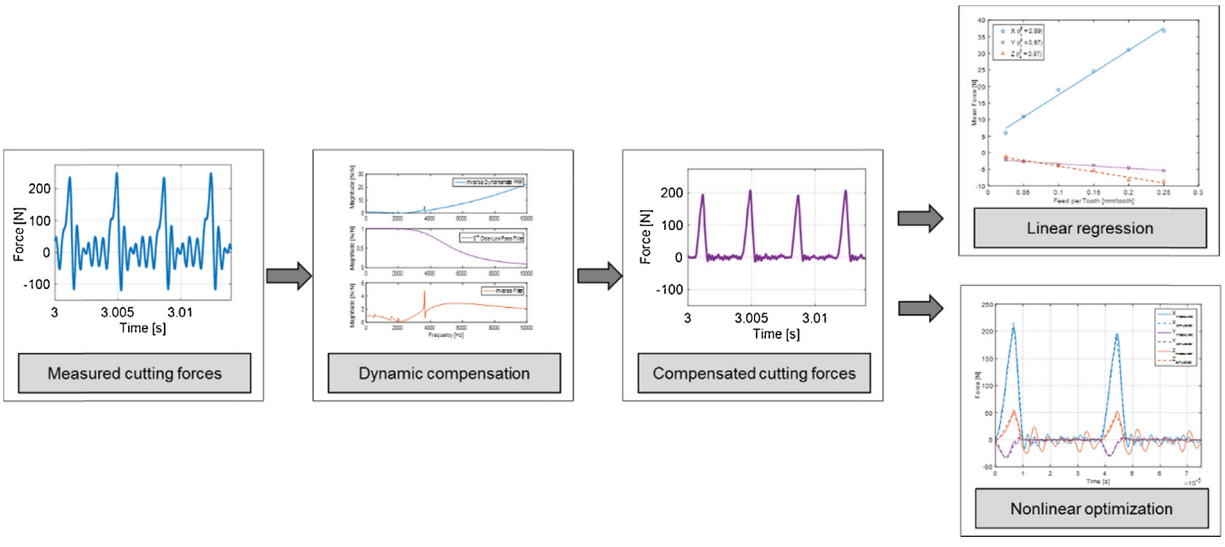

Fig. 4. Flow diagram detailing the experimental method used in this study.

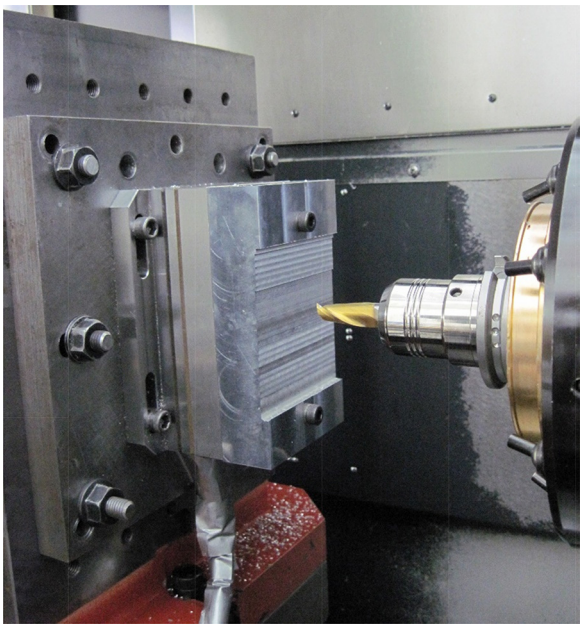

Fig. 5. Setup for cutting force measurements using a three-axis dynamometer.

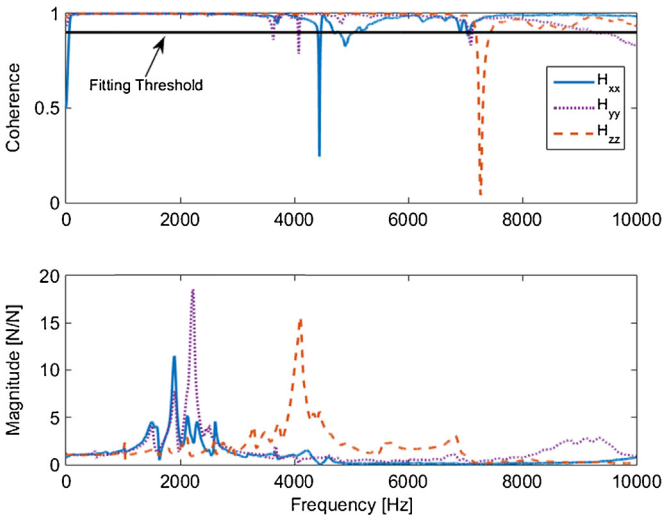

Fig. 6. Example measurement results of a dynamometer force-to-force FRF in the *xyz* directions including the coherence and magnitude.

was aligned to the machine axes using a test indicator. A charge amplifier (Kistler Type 5010), signal analyzer (Data Translation DT9837B), and data acquisition software (Spinscope Manufacturing Laboratories, Inc.) were used to record the cutting force.

The cutting tool used in this study was a 12.7 mm diameter solid carbide endmill (SGS 39363) with a 30° helix angle. It was clamped in a Schunk SINO-R tool holder with approximately 40 mm of overhang. Cutting tests were performed with the tool in two conditions: (1) two flutes; and (2) single flute (i.e., one flute removed).

Cutting tests were performed under stable milling conditions with an axial depth of cut of 3 mm. Other process parameters, such as radial depth of cut, spindle speed, feed per tooth, and milling direction (i.e., up/down milling), were varied. Details of the cutting force tests are listed in Table 1. Each cutting force measurement was repeated three times to enable a statistical analysis while minimizing the effect of tool wear on the measured cutting forces.

3.2. Dynamic compensation of measured cutting forces

Accurate measurement of cutting forces is crucial for machining process simulation and for evaluation of cutting tool geometries and concepts [16]. The most common method of cutting force measurement found in the literature use commercial piezoelectric dynamometers. Because these dynamometers are not infinitely rigid, they may be considered as a dynamic system with a characteristic frequency response which defines the measurement bandwidth of the instrument. As the tooth passing frequency and subsequent harmonics begin to approach the resonant frequencies of the dynamometer, unwanted frequency content is superimposed on the cutting force signal. The resulting measured forces suffer from poor accuracy, and, therefore, the process of cutting force coefficient determination at high tooth passing frequencies (i.e., high spindle speeds) is complicated.

In this study, a compensation technique based on inverse FRF filtering was implemented to attenuate the unwanted frequency content in the measured cutting forces. The filter was constructed by inverting the measured force-to-force FRF of the dynamometer [16], also commonly referred to as the force transmissibility.

$$H(\omega) = \frac{F_{out}(\omega)}{F_{in}(\omega)} \tag{20}$$

The dynamometer force-to-force FRF is a complex-valued ratio of the output force from the dynamometer, $F_{out}(\omega)$, and the input force from the cutting process, $F_{in}(\omega)$, in the frequency domain. Ideally, there is no unwanted frequency content added to the measured forces. In this case the magnitude of the dynamometer FRF would be one at all frequencies. Because the dynamometer/workpiece system has finite mass, stiffness, and damping, the magnitude and phase of the measured cutting forces depart from their ideal values.

In [15], Castro et al. use a 3×3 FRF matrix, referred to as the dynamometer's transmissibility matrix, which contains three direct FRFs (i.e., the dynamometer force output is in the same *xyz* component direction as the applied force) and six cross FRFs (i.e., the dynamometer force output is in the *xyz* component directions orthogonal to the applied force). The inclusion of the cross FRFs in the inverse filtering technique serves to attenuate frequency content from the measured cutting forces due to crosstalk in the dynamometer's *xyz* component directions. In this study, the effect of crosstalk (i.e., cross FRFs) was considered to be negligible.

The success of the inverse filtering method is primarily limited by the accuracy and bandwidth of the measured dynamometer/workpiece system FRF and by the fitting of the measured FRF to compute modal parameters which are used to mathematically reconstruct the compensation filter. Typically, the measurement accuracy is assessed by computing the coherence, which serves as a quality index between the input force and the dynamometer output. Aside from the cases where coherence is poor in close proximity to anti-resonance frequencies, a coherence value of 0.90 was selected as the threshold value for fitting the measured FRF; see Fig. 6.

Fitting of the measured FRF, which is used to compute the system's modal parameters, is completed using a two-stage process which includes: (1) the peaking picking method; and (2) a nonlinear optimization. The peak-picking method [10] is used to perform a preliminary fit to the FRF. Because of modal truncation, where modes are present outside of the measurement bandwidth and contribute to the dynamic response of the dynamometer, but are not included in the fit, the accuracy of the FRF fit suffers. To compensate for this effect and improve the accuracy of the fit, a nonlinear optimization of the FRF's magnitude is performed. Example results from the FRF fitting process are displayed in Fig. 7.

The magnitude of the inverted, dynamometer FRF decays to near-zero at high frequencies; see Fig. 6. Applying a filter that is simply the inversion of the dynamometer FRF will lead to

Table 1
Milling process parameters selected for cutting force measurements.

Cut direction	Radial immersion [%]	Spindle speed [krpm]	Feed [mm/tooth]
Up milling	10	8	(0.025, 0.05, 0.10, 0.15, 0.20, 0.25)
Down milling	10	8	(0.025, 0.05, 0.10, 0.15, 0.20, 0.25)
Down milling	10	(1, 2, 3, 4, 6, 8, 10, 12.5, 15, 17.5, 20)	0.10
Down milling	(10,30,50)	8	0.10

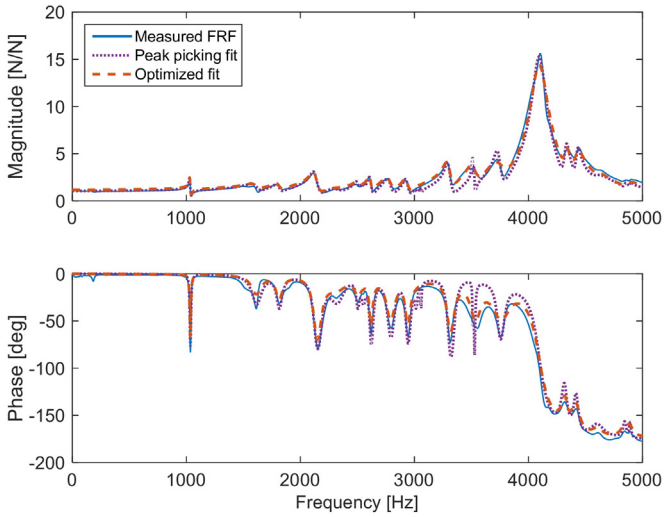

Fig. 7. Example results from the two-stage modal fit of a measured dynamometer FRF.

amplification of high frequency measurement noise as shown in Fig. 8a. This is avoided by convolving the inverted dynamometer FRF with a fourth-order lowpass filter; see Fig. 8b. The cutoff frequency of the lowpass filter is selected such that the magnitude response of the final, inverse FRF filter is near unity at high frequencies. The resulting inverse FRF filter, shown in Fig. 8c, simultaneously amplifies and truncates the relevant frequency components, which are distorted by the dynamic response of the dynamometer, while preserving the high frequency components of the measured cutting forces. Preservation of the high frequency components of the measured cutting forces is crucial for evaluating the stability of milling operations.

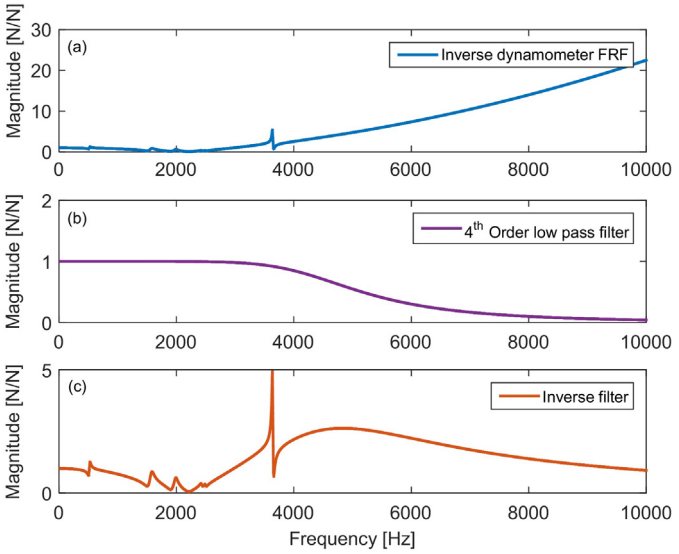

Fig. 8. Magnitude response of (a) the inverted, measured dynamometer FRF, (b) second order lowpass filter, and (c) inverse FRF filter.

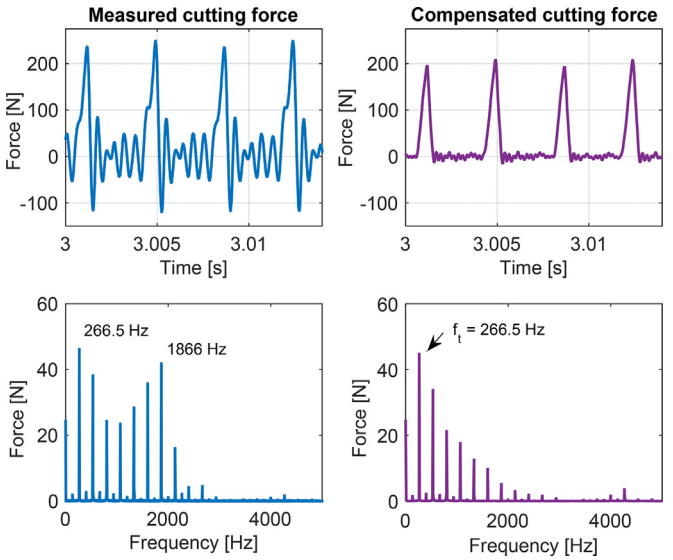

Fig. 9. Example results of the dynamic compensation on the time domain (top) and frequency domain (bottom) cutting forces.

Typical results from the dynamic compensation technique are provided in Fig. 9. The measured cutting forces contain significant dynamic distortion as evidenced by the amplification of the frequency content in the measured cutting forces near 1866 Hz. This frequency corresponds to the largest magnitude of the *x*-direction dynamometer force-to-force FRF as shown in Fig. 6. The compensated cutting forces exhibit frequency content at the tooth passing frequency, f_{tooth}, which occurs at 266.5 Hz for the milling operation using a two flute endmill with a spindle speed of 8000 rpm. Frequency content is also observed at harmonics of the tooth passing frequency as well as the runout frequency which occurs at one-half of the tooth passing frequency.

Because the instantaneous force, nonlinear optimization method simulates cutting forces in the time domain as a function of cutter rotation angle, the *x*, *y*, and *z* component forces have a phase relationship. Introduction of a relative phase shift, due to the response of the inverted dynamometer FRF, to the measured *x*, *y*, and *z* component forces is undesirable as it will lead to errors in the instantaneous force, nonlinear optimization method results. Typical results from the dynamic compensation technique are shown in Fig. 10 for the *x*, *y*, and *z* component forces in the time domain. No phase shift of the component forces relative to one another is observed.

3.3. Validation testing

The validity of the instantaneous force, nonlinear optimization method of calibrating the mechanistic force model is evaluated in the framework of milling stability experiments. The feed per tooth dependence of the specific force coefficients was evaluated experimentally by performing a series of milling cuts on a system with fixed dynamics. The milling cuts were performed at the same axial depth of cut-spindle speed combinations while varying the feed per tooth. Stability predictions were performed using

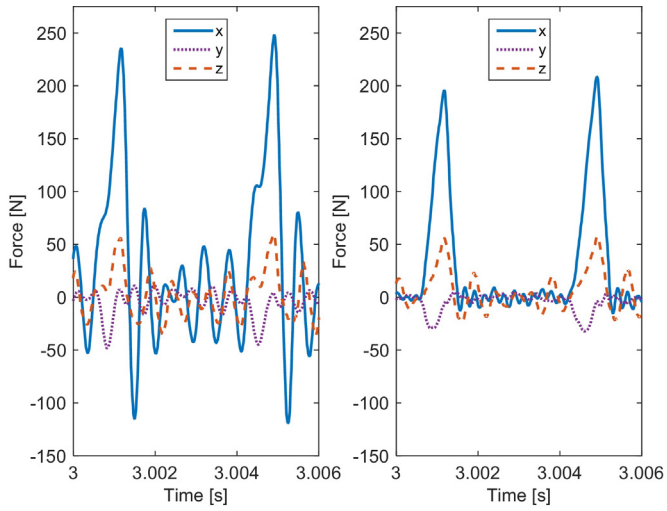

Fig. 10. Example results of the dynamic compensation (right) on the *x*, *y*, and *z* components of the measured cutting forces (left).

peak-to-peak (PTP) force diagrams, which are generated by multiple runs of a time domain simulation. The time domain simulation model is based on the "Regenerative Force, Dynamic Deflection Model" described by Smith and Tlusty in [28]. Additional details of the time domain simulation are given in [10] and the PTP force diagram is presented by Smith et al. in [29].

In order to facilitate the evaluation of stability in the validation tests, the system dynamics were controlled via a single degree-of-freedom, parallelogram type flexure, shown in Fig. 11. The flexure provides a convenient method for evaluating the stability of the milling process by, ideally, constraining vibration to a single, flexible direction. Modal parameters for the combined flexure/workpiece system were obtained via impact testing using a modal hammer (PCB 086C04) to provide the excitation force and a low mass accelerometer (PCB 352C23) to record the response. Table 2 lists the natural frequency, f_n, modal stiffness, k, and dimensionless, viscous damping ratio, ζ, for the single degree-of-freedom flexure in the feed direction (i.e., x).

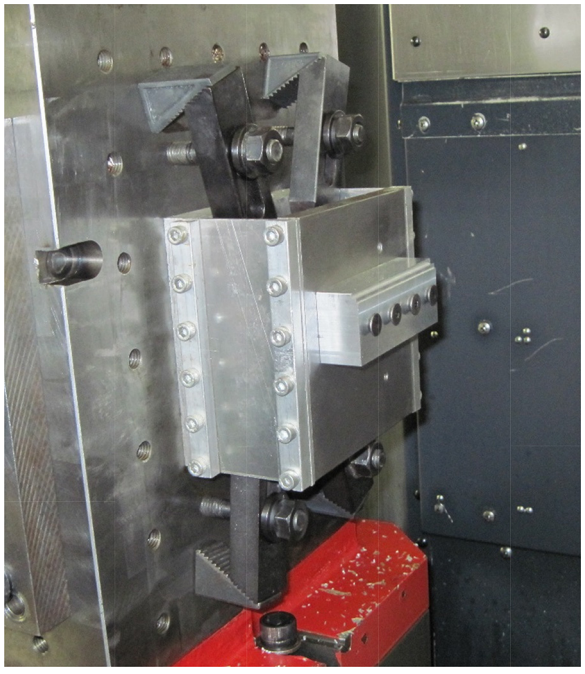

Fig. 11. Setup for validation testing. The parallelogram type flexure and attached workpiece are mounted to the machine tool's tombstone.

Table 2
Modal parameters for flexure in the x (feed) direction.

f_n [Hz]	k [N/m]	ζ
236.7	5.03×10^6	0.0097

The validation tests were performed using the same cutting tool previously detailed (SGS 39363). A low mass accelerometer (PCB 352C23) was used to measure the acceleration of the flexure/workpiece system during cutting. The frequency content of the acceleration signal was used to distinguish between stable and unstable milling conditions. Unstable milling operations were characterized by acceleration signals containing significant frequency content at or near the flexure's natural frequency, while stable milling conditions contained only frequency content at the tooth passing frequency and its harmonics.

4. Experiment results

4.1. Feed per tooth dependence

The following experimental results compare the specific force coefficients calculated using the average force, linear regression and instantaneous force, nonlinear optimization methods over a range of feed per tooth values. The cutting force measurements were repeated three times for each of the selected feed per tooth values, which are given in Table 1.

Fig. 12 shows the result of the average force, linear regression analysis of the measured cutting forces over the range of feed per tooth values. A satisfactory fit was achieved as indicated by the coefficients of determination, r^2. The reported, measured cutting forces reflect the average forces calculated over the three repeated measurements. The calculated specific force coefficients are given in Table 3.

The cutting force coefficients, determined using the instantaneous force, nonlinear optimization method, over the range of selected feed per tooth values are given in Fig. 13. The mean value of the three repeat measurements are reported along with the 95% confidence interval which was calculated using the t-distribution. It is observed that the tangential and normal cutting force

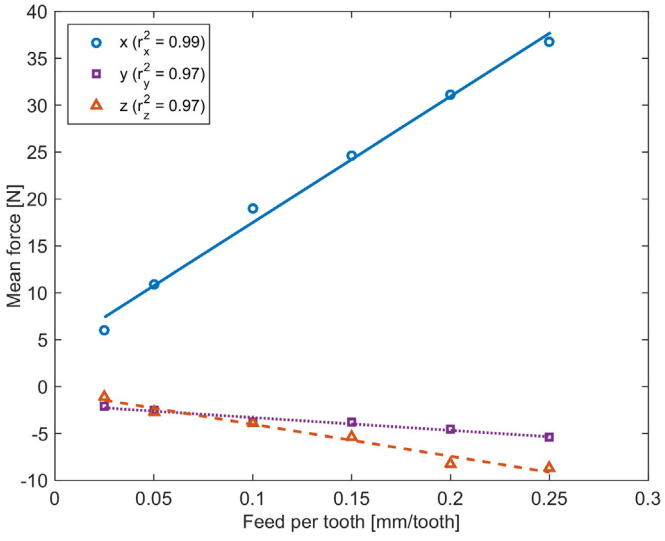

Fig. 12. Average force, linear regression results from the 10% radial immersion up milling cut conducted at a spindle speed of 8000 rpm.

Table 3
Specific force coefficients calculated using the average force, linear regression method for the 10% radial immersion up milling cut conducted at a spindle speed of 8000 rpm.

Cutting force coefficients [N/mm^2]		Edge force coefficients [N/mm]	
k_{tc}	805	k_{te}	6
k_{nc}	418	k_{ne}	6
k_{ac}	227	k_{ae}	1

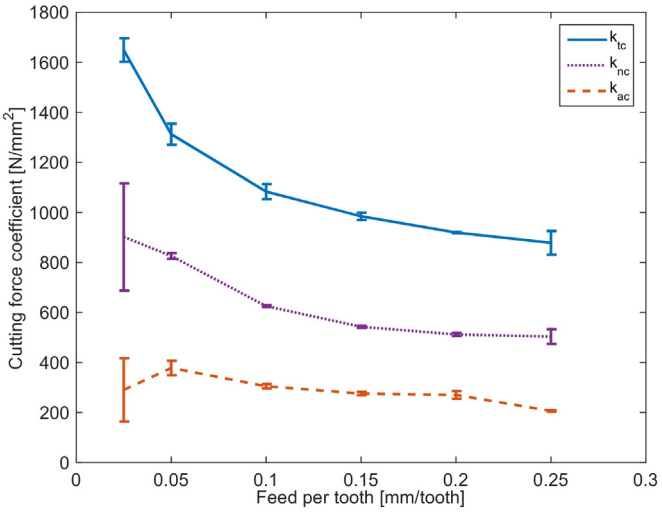

Fig. 13. Cutting force coefficients calculated using the instantaneous force, nonlinear optimization method for a 10% radial immersion up milling cut conducted at a spindle speed of 8000 rpm.

coefficients vary nonlinearly with feed per tooth as reported by other researchers [13]. No observable trend was noted in the edge force coefficients.

A series of cutting tests were performed with identical milling parameters (i.e., spindle speed, axial depth of cut, radial immersion), but in the down milling direction. The resulting specific force coefficients calculated using the average force, linear regression and instantaneous force, nonlinear optimization methods are presented in Table 4 and Fig. 14, respectively. It is observed that the force coefficients for the different milling directions are in good agreement.

The instantaneous, uncut chip thickness as seen by the cutting tool as each flute engages in the cut is influenced by both the commanded feed per tooth and percent radial immersion. For example, if the commanded feed per tooth is held fixed and percent radial immersion is decreased, the instantaneous, uncut chip thickness also decreases. To study the effects of radial immersion on the specific force coefficients, a series of cutting tests were performed at 10%, 30%, and 50% radial immersion, while holding other milling parameters fixed. The resulting tangential cutting force coefficients, calculated using the instantaneous force, nonlinear optimization method, are reported in Fig. 15 along with the 95% confidence intervals. A statistically significant variation in the tangential cutting force coefficient as a function of radial immersion may be observed.

Table 4
Specific force coefficients calculated using the average force, linear regression method for the 10% radial immersion down milling cut conducted at a spindle speed of 8000 rpm.

Cutting force coefficients [N/mm^2]		Edge force coefficients [N/mm]	
k_{tc}	786	k_{te}	11
k_{nc}	417	k_{ne}	11
k_{ac}	158	k_{ae}	1

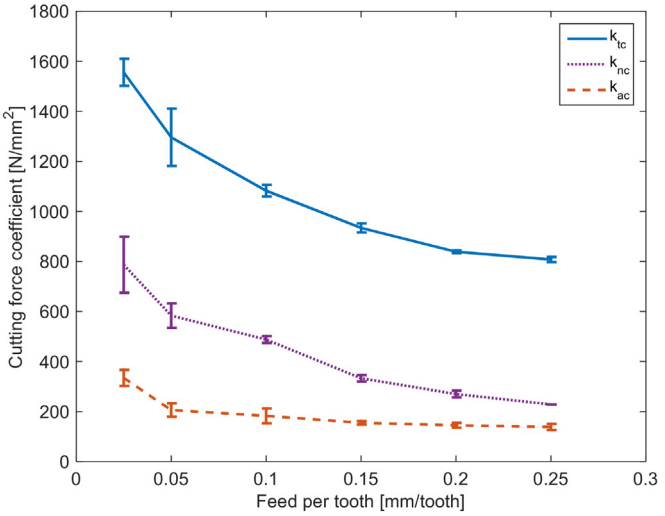

Fig. 14. Cutting force coefficients calculated using the instantaneous force, nonlinear optimization method for a 10% radial immersion down milling cut conducted at a spindle speed of 8000 rpm.

A similar trend in the normal direction coefficient was observed. However, an overlap of the 95% confidence interval precluded a statistically significant result.

4.2. Cutting speed dependence

A series of cutting tests were performed over a range of spindle speeds and the force coefficients were calculated using the instantaneous force, nonlinear optimization method. The averaged results and 95% confidence intervals are displayed in Fig. 16. The resulting trend is in good agreement with results published by Grossi et al. [30,31]. It is noteworthy that there is a general downward trend in the force coefficients until the critical spindle speed of approximately 12,500 rpm. Beyond this critical spindle speed, there is a general upward trend. Typically the downward trend is attributed to thermal softening of the workpiece material due to the increased temperature at the tool/chip interface at high cutting speeds.

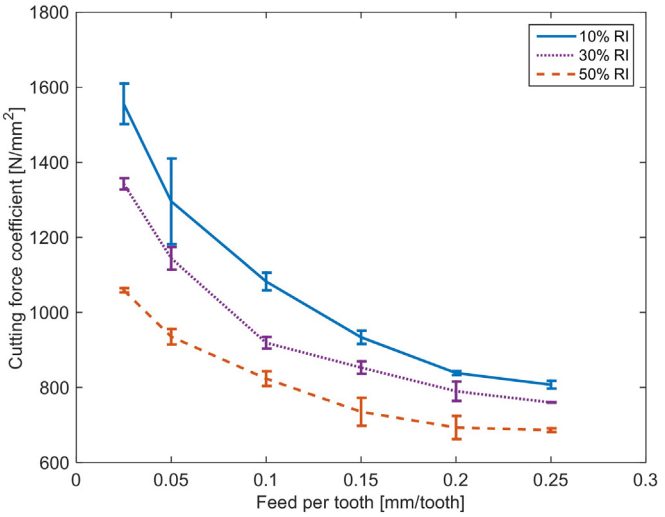

Fig. 15. The tangential cutting force coefficient, calculated by the instantaneous force, nonlinear optimization method, as a function of radial immersion.

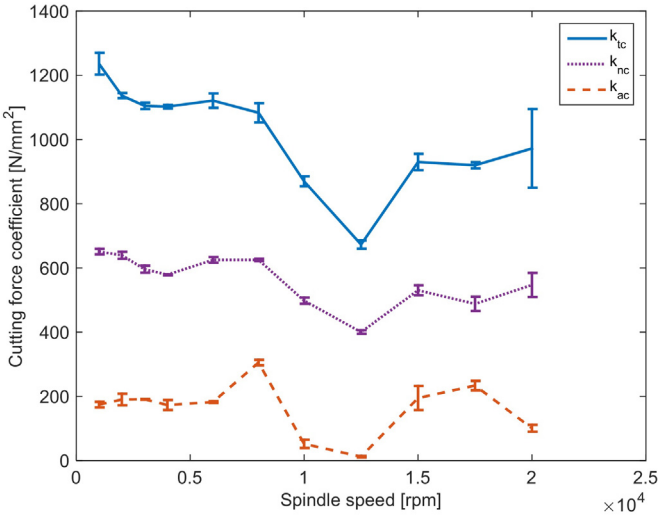

Fig. 16. Cutting force coefficients calculated using the instantaneous force, nonlinear optimization method over the range of selected spindle speeds for the 10% radial immersion down milling operation.

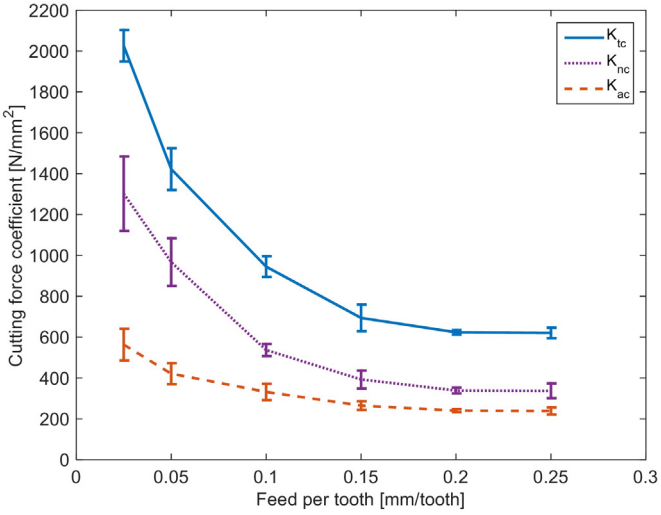

Fig. 17. Cutting force coefficients calculated using the instantaneous force, nonlinear optimization method for a 10% radial immersion down milling cut conducted at a spindle speed of 8000 rpm.

4.3. Validation testing

Validation testing was conducted at two feed per tooth values, 0.05 mm/tooth and 0.25 mm/tooth, for a 10% radial immersion down milling cut. The cutting force coefficients were calculated using the instantaneous force, nonlinear optimization method. The results are provided in Fig. 17 and Table 5 It was determined that the endmill exhibited approximately 30 μm of flute-to-flute runout. At low feed per tooth values (i.e., 0.025 mm/tooth) only one tooth was engaged in the cut per revolution and, as a result, the cutting force coefficients are higher at low feed per tooth values than reported for other cutting tools of similar geometry.

Table 5
Cutting force coefficients used for milling stability predictions using the PTP force diagram.

Feed per tooth [mm/tooth]	Cutting force coefficients [N/mm^2]		Edge force coefficients [N/mm]	
0.05	k_{tc}	1422	k_{te}	16
	k_{nc}	967	k_{ne}	13
	k_{ac}	421	k_{ae}	0
0.25	k_{tc}	620	k_{te}	34
	k_{nc}	337	k_{ne}	20
	k_{ac}	239	k_{ae}	0

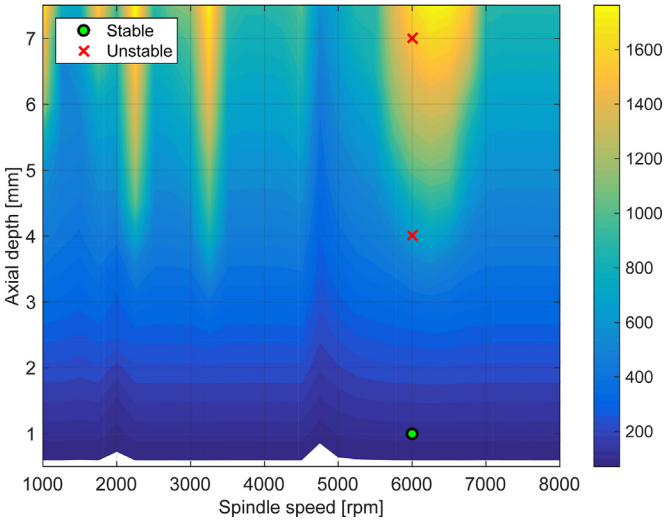

Fig. 18. PTP force diagram generated using the specific force coefficients calculated for a feed rate of 0.05 mm/tooth. Stable (circle) and unstable (cross) validation test results are shown.

The PTP force diagram is conceptually similar to the traditional stability lobe diagram in the sense that it provides a map of stable and unstable axial depth of cut-spindle speed combinations. It conveys this information as a contour map of PTP cutting forces generated from numerous time domain simulations. Because the time domain simulations do not make the simplifying assumptions used to generate analytical stability lobe diagrams for milling and they capture nonlinearities in the milling process, they are particularly well suited for predicting stable milling conditions at low radial immersion. The time domain simulation takes into account the tool and workpiece dynamics in three orthogonal directions as well as various parameters such as flute-to-flute runout and helix angle. The PTP force diagram generated using the specific force coefficients for a feed rate of 0.05 mm/tooth is shown in Fig. 18. The results of the validation test cuts are included.

The resulting PTP force diagram generated using the specific force coefficients for a feed rate of 0.25 mm/tooth is shown in Fig. 19. The results of the validation test cuts are included. It was observed that in both cases the PTP force diagram accurately predicted stable and unstable axial depth of cut-spindle speed combinations. Furthermore it is observed that the validation tests conducted at a 4 mm axial depth of cut yielded different results. The lower feed rate cut produced unstable results while the higher feed rate cut was stable.

5. Discussion

In this paper, a comparative study that examined the dependence of specific cutting force coefficients on milling process parameters such as feed per tooth, spindle speed, and radial immersion was presented. The mechanistic force model was detailed and the methods for calibrating the model (i.e., determining the specific force coefficients) were presented. Additionally, the dynamic compensation method was detailed which extended the bandwidth over which cutting forces could be measured using a commercial dynamometer. Next, the specific force coefficients, calculated using the average force, linear regression and instantaneous force, nonlinear optimization methods, for a range of milling process

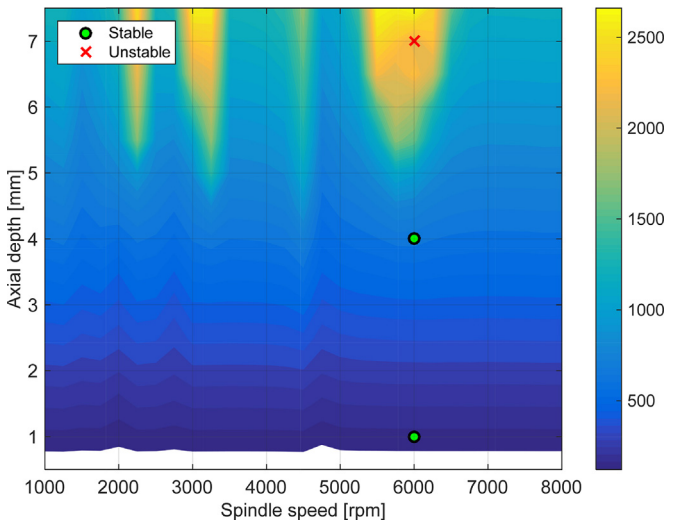

Fig. 19. PTP force diagram generated using the specific force coefficients calculated for a feed rate of 0.25 mm/tooth. Stable (circle) and unstable (cross) validation test results are shown.

parameters were reported. Finally, the instantaneous force, nonlinear optimization method was validated in the framework of milling stability tests.

It was determined that low feed rates, which are often recommended for hard-to-machine materials, produce disproportionately larger cutting forces per uncut chip area than high feed rates, particularly for low radial immersion milling. From a practical standpoint, this becomes relevant for the finish milling of titanium performs, which are often encountered in the aerospace industry. The results reported here suggest that high feed rates increase the critical axial depth of cut below which all spindle speeds yield stable milling operations.

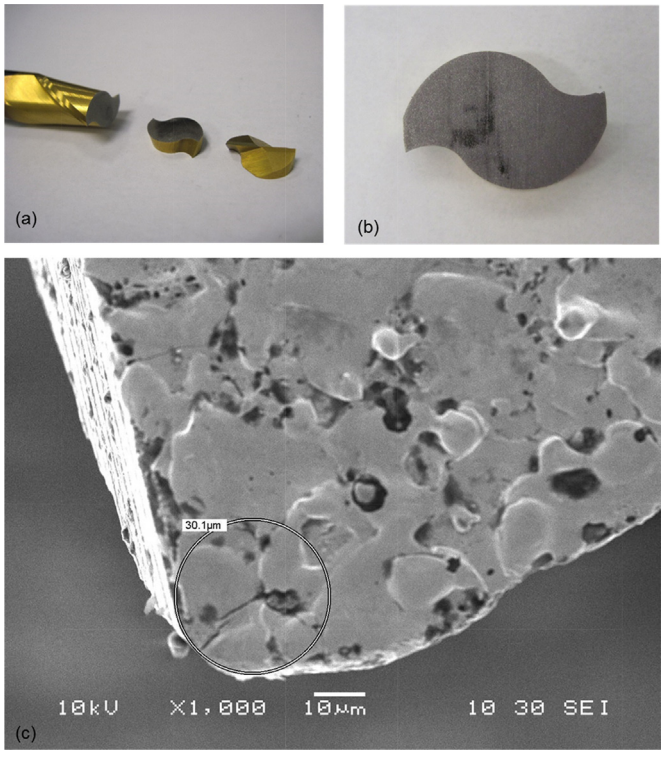

Fig. 20. A milling tool (a) cut into axial disks (b) to facilitate cutting edge radius measurements with an SEM (c). In (c) the flank face is on the left and the rake race is on the right.

With respect to chip formation, the rake angle (i.e., inclination of the cutting edge relative to the surface normal) depends on both the commanded feed per tooth and the radius of the milling tool's cutting edge radius. Although the cutting tool may have a positive rake angle at the macroscopic scale, as the commanded feed per tooth approaches the same order of magnitude as the cutting edge radius of the milling tool, shown in Fig. 20, the effective rake angle becomes negative. This change in rake angle is accompanied by a change in the mechanism by which the chip is formed. Additionally, the negative rake angle serves to impose compressive stresses on the workpiece surface. These factors contribute to the increase in the cutting force coefficients at low values of feed per tooth. In Fig. 20, where the cutting tool's rake face is to the right of the cutting edge, it is observed that although the cutting edge radius is on the order of approximately 30 μm, the length of the negative rake angle may be several time larger.

Appendix A. Arbitrary radial immersion cutting force coefficient solution

For the general case of arbitrary radial immersion, the six cutting force coefficients of the mechanistic cutting force model from Section 2 may be solved as follows. Expanding Eqs. (5)–(7) and arranging them in slope–intercept form gives:

$$\bar{F}_x = \frac{N_t b}{8\pi}\{k_t[\cos(2\emptyset_s) - \cos(2\emptyset_e)] + k_n[(2\emptyset_e - \sin(2\emptyset_e)) - (2\emptyset_s - \sin(2\emptyset_s))]\}f_t + \frac{N_t b}{2\pi}\{k_{te}[\sin(\emptyset_e) - \sin(\emptyset_s)] + k_{ne}[\cos(\emptyset_s) - \cos(\emptyset_e)]\} \quad (21)$$

$$\bar{F}_y = \frac{N_t b}{8\pi}\{k_t[(2\emptyset_e - \sin(2\emptyset_e)) - (2\emptyset_s - \sin(2\emptyset_s))] + k_n[\cos(2\emptyset_e) - \cos(2\emptyset_s)]\}f_t + \frac{N_t b}{2\pi}\{k_{te}[\cos(\emptyset_s) - \cos(\emptyset_e)] + k_{ne}[\sin(\emptyset_s) - \sin(\emptyset_e)]\} \quad (22)$$

$$\bar{F}_z = \frac{N_t b}{2\pi}\{k_a[\cos(\emptyset_e) - \cos(\emptyset_s)]\}f_t + \frac{N_t b}{2\pi}\{k_{ae}[\emptyset_s - \emptyset_e]\} \quad (23)$$

where the coefficient multiplying feed per tooth is the slope and the remaining term is the intercept. Arranging the expressions in matrix form yields:

$$\begin{bmatrix} b_{11} & \cdots & b_{16} \\ \vdots & \ddots & \vdots \\ b_{61} & \cdots & b_{66} \end{bmatrix} \begin{Bmatrix} k_{tc} \\ k_{te} \\ k_{nc} \\ k_{ne} \\ k_{ac} \\ k_{ae} \end{Bmatrix} = \begin{Bmatrix} a_{1x} \\ a_{0x} \\ a_{1y} \\ a_{0y} \\ a_{1z} \\ a_{0z} \end{Bmatrix} \quad (24)$$

where:

$$b_{11} = \frac{N_t b}{8\pi}[\cos(2\phi_s) - \cos(2\phi_e)] \quad (25)$$

$$b_{13} = \frac{N_t b}{8\pi}[(2\phi_e - 2\phi_s) + (\sin(2\phi_s) - \sin(2\phi_e))] \quad (26)$$

$$b_{22} = \frac{N_t b}{2\pi}[\sin(\phi_e) - \sin(\phi_s)] \quad (27)$$

$$b_{24} = \frac{N_t b}{2\pi}[\cos(\phi_s) - \cos(\phi_e)] \quad (28)$$

$$b_{31} = \frac{N_t b}{8\pi}[(2\phi_e - 2\phi_s) + (\sin(2\phi_s) - \sin(2\phi_e))] \tag{29}$$

$$b_{33} = \frac{N_t b}{8\pi}[\cos(2\phi_e) - \cos(2\phi_s)] \tag{30}$$

$$b_{42} = \frac{N_t b}{2\pi}[\cos(\phi_s) - \cos(\phi_e)] \tag{31}$$

$$b_{44} = \frac{N_t b}{2\pi}[\sin(\phi_s) - \sin(\phi_e)] \tag{32}$$

$$b_{55} = \frac{N_t b}{2\pi}[\cos(\phi_e) - \cos(\phi_s)] \tag{33}$$

$$b_{66} = \frac{N_t b}{2\pi}(\phi_s - \phi_e) \tag{34}$$

All other elements are equal to zero. The vector of specific force coefficients can be determined using:

$$\begin{Bmatrix} k_{tc} \\ k_{te} \\ k_{nc} \\ k_{ne} \\ k_{ac} \\ k_{ae} \end{Bmatrix} = \begin{bmatrix} b_{11} & \cdots & b_{16} \\ \vdots & \ddots & \vdots \\ b_{61} & \cdots & b_{66} \end{bmatrix}^{-1} \begin{Bmatrix} a_{1x} \\ a_{0x} \\ a_{1y} \\ a_{0y} \\ a_{1z} \\ a_{0z} \end{Bmatrix} \tag{35}$$

References

[1] Ehmann KFKSG, DeVor RE, Lazoglu I. Machining process modeling: a review. J Manuf Sci Eng 1997;119:655–63.
[2] van Luttervelt CA, Childs THC, Jawahir IS, Klocke F, Venuvinod PK, Altintas Y, et al. Present situation and future trends in modelling of machining operations progress report of the CIRP working group 'Modelling of machining operations'. CIRP Ann Manuf Technol 1998;47(2):587–626.
[3] Merchant ME. Basic mechanics of the metal cutting process. J Appl Mech 1944;11(A):168–75.
[4] Amarego EJA, Brown RH. The machining of metals. Prentice-Hall; 1969.
[5] Mackerle J. Finite element analysis and simulation of machining: an addendum: a bibliography (1996–2002). Int J Mach Tools Manuf 2003;43:103–14.
[6] Martellotti M. An analysis of the milling process. Trans ASME 1941;63(2).
[7] Sabberwal FKAJP. An investigation into the cutting force pulsations during milling operations. Int J Mach Tool Des Res 1961;1:15–33.
[8] Sabberwal AJP. Chip section and cutting force during the milling operation. CIRP Ann Manuf Technol 1962;10(3).
[9] Budak E, Altintas Y, Armarego E. Prediction of milling force coefficients from orthogonal cutting data. J Manuf Sci Eng 1996;118(2):216–24.
[10] Schmitz TL, Smith KS. Machining dynamics: frequency response to improved productivity. Springer Science & Business Media; 2008.
[11] Altintas Y. Manufacturing automation: metal cutting mechanics, machine tool vibrations, and CNC design. Cambridge University Press; 2012.
[12] Gonzalo O, Beristain J, Jauregi H, Sanz C. A method for the identification of the specific force coefficients for mechanistic milling simulation. Int J Mach Tools Manuf 2010;50(9):765–74.
[13] Campatelli G, Scippa A. Prediction of milling cutting force coefficients for aluminum 6082-T4. Procedia CIRP 2012;1:563–8.
[14] Altintas Y, Park SS. Dynamic compensation of spindle-integrated force sensors. CIRP Ann Manuf Technol 2004;53(1):305–8.
[15] Ricardo Castro L, Viéville P, Lipinski P. Correction of dynamic effects on force measurements made with piezoelectric dynamometers. Int J Mach Tools Manuf 2006;46(14):1707–15.
[16] Magnevall M, Lundblad M, Ahlin K, Broman G. High frequency measurements of cutting forces in milling by inverse filtering. Mach Sci Technol 2012;16(4):487–500.
[17] Chae J, Park S. High frequency bandwidth measurements of micro cutting forces. Int J Mach Tools Manuf 2007;47:1433–41.
[18] Albrecht A, Park S, Altintas Y, Pritschow G. High frequency bandwidth cutting force measurement in milling using capacitance displacement sensors. Int J Mach Tools Manuf 2005;45:993–1008.
[19] Kang I, Kim J, Hong C, Kim J. Development and evaluation of tool dynamometer for measuring high frequency cutting forces in micro milling. Int J Precis Eng Manuf 2010;11(6):817–21.
[20] Girardin F, Remond D, Rigal J-F. High frequency correction of dynamometer for cutting force observation in milling. ASME J Manuf Sci Eng 2010;132(031002):1–8.
[21] Castro L, Viville P, Lipinski P. Correction of dynamic effects on force measurements made with piezoelectric dynamometers. Int J Mach Tools Manuf 2006;46:1707–15.
[22] Tounsi N, Otho A. Dynamic cutting force measuring. Int J Mach Tools Manuf 2000;40:1157–70.
[23] Jun MB, Ozdoganlar OB, DeVor RE, Kapoor SG, Kirchheim A, Schaffner G. Evaluation of a spindle-based force sensor for monitoring and fault diagnosis of machining operations. Int J Mach Tools Manuf 2002;42:741–51.
[24] Korkmaz E, Bediz B, Gozen BA, Ozdoganlar OB. Dynamic characterization of multi-axis dynamometers. Precis Eng 2014;38:148–61.
[25] Schmitz TL, Couey J, Marsh E, Mauntler N, Hughes D. Runout effects in milling: surface finish, surface location error, and stability. Int J Mach Tools Manuf 2007;47(5):841–51.
[26] Feng H-Y, Menq C-H. The prediction of cutting forces in the ball end milling process. Int J Mach Tools Manuf 1994;34(5):667–710.
[27] Coleman TF, Li Y. On the convergence of interior-reflective Newton methods for nonlinear minimization subject to bounds. Math Program 1994;67:189–224.
[28] Smith S, Tlusty J. An overview of modeling and simulation of the milling process. J Eng Ind 1991;113(2):169–75.
[29] Smith S, Tlusty J. Efficient simulation programs for chatter in milling. CIRP Ann Manuf Technol 1993;42(1):463–6.
[30] Grossi N, Sallese L, Scippa A, Campatelli G. Chatter stability prediction in milling using speed-varying cutting force coefficients. Procedia CIRP 2014;14:170–5.
[31] Grossi N, Sallese L, Scippa A, Campatelli G. Speed-varying cutting force coefficient identification in milling. Precis Eng 2015;42:321–34.